Bose-Einstein correlations of soft pions in ultrarelativistic nucleus-nucleus collisions

WA80 Collaboration

INSTITUT FÜR KERNPHYSIK

UNIVERSITÄT MÜNSTER

Bose-Einstein correlations of soft pions in ultrarelativistic nucleus-nucleus collisions

WA80 Collaboration

T.C. Awes[5], M.A. Bloomer[2], C. Blume[4], D. Bock[4], R. Bock[1], D. Bucher[4], G. Clewing[4], S. Garpman[3], R. Glasow[4], H.Å. Gustafsson[3], H.H. Gutbrod[1], G. Hölker[4], J. Idh[3], P. Jacobs[2], K.H. Kampert[4], B.W. Kolb[1], H. Löhner[6], F.E. Obenshain[5], A. Oskarsson[3], I. Otterlund[3], T. Peitzmann[4], F. Plasil[5], A.M. Poskanzer[2], M. Purschke[1], B. Roters[1], S. Saini[5], R. Santo[4], H.R. Schmidt[1], S.P. Sørensen[5,7], K. Steffens[4], P. Steinhaeuser[1], E. Stenlund[3], D. Stüken[4] and G.R. Young[5]

1. *Gesellschaft für Schwerionenforschung, D-64291 Darmstadt, Fed. Rep. of Germany*
2. *Lawrence Berkeley Laboratory, Berkeley, California 94720, USA*
3. *University of Lund, S-22362 Lund, Sweden*
4. *University of Münster, D-48149 Münster, Fed. Rep. of Germany*
5. *Oak Ridge National Laboratory, Oak Ridge, Tennessee 37831, USA*
6. *KVI, University of Groningen, NL-9747 AA Groningen, Netherlands*
7. *University of Tennessee, Knoxville, Tennessee 37996, USA*

Abstract

A detailed analysis of pair correlations of positive pions in the target rapidity region is presented. Data on 200 A GeV nuclear collisions were measured with the Plastic Ball in the WA80 experiment at the CERN SPS. The correlation functions are compared with analytical functions and with simulations incorporating Bose-Einstein symmetrization, final-state interactions and detector resolution. Source radii are shown to increase with increasing target size and with centrality. For central collisions the radii are larger than the geometrical sizes of the involved nuclei.

1 Introduction

Pion interferometry has become a widespread tool in high energy nuclear and particle physics. It allows a study of the space-time properties of the particle emitting source via the enhancement in the production of identical pions with similar momentum [1]. The underlying effects are also known as Bose-Einstein Correlations, the Hanbury-Brown - Twiss effect (HBT) [2] or the Goldhaber - Goldhaber - Lee - Pais effect (GGLP) [3].

1

A simple theoretical picture of multi-particle production yields the following prediction for the two-particle correlation function [1]:

$$C_2 \equiv \frac{<n>^2}{<n(n-1)>} \cdot \frac{d^6 N/dp_1^3 dp_2^3}{d^3 N/dp_1^3 \cdot d^3 N/dp_2^3} = 1 + \lambda \cdot |\tilde{\rho}(p_1^\mu - p_2^\mu)|^2, \quad (1)$$

where n is the pion multiplicity and $d^3 N/dp_i^3$ and $d^6 N/dp_1^3 dp_2^3$ are the one-pion and two-pion inclusive yields. $\tilde{\rho}$ is the Fourier transform of the distribution of emitters; the most commonly chosen analytic expressions for $\tilde{\rho}$ contain a suitable correlation length R.

The parameter λ, a correlation strength, was introduced for technical reasons [4]; it is expected to be $= 1$ for a completely chaotic source. Theoretically a value of $\lambda < 1$ can be ascribed to a certain amount of coherent production of pions [5], but in the experiment many different effects may reduce the measured value of λ [6, 7].

Experiments with ultrarelativistic nuclei have revealed the importance of rescattering of produced particles in the target spectator matter [8, 9]. Hints for pion absorption in the target nucleus are observed [10]. It is therefore of interest to study the target fragmentation region also by interferometric methods. First WA80 results from pion interferometry analysis in the target region for ^{16}O-induced reactions have been published previously [11]. In the present paper the analysis will be extended to other projectiles - reactions of 200 AGeV p, ^{16}O and ^{32}S with various targets will be studied. In addition, a pair efficiency correction is introduced, which allows to measure pairs of smaller relative momentum than compared to [11]. This efficiency results from cross-talk via scattering of the decay-positrons into neighboring modules and has been determined from the data. First results of fits using this efficiency correction have been presented earlier [12, 13].

2 Data Analysis

Data presented here have been taken in the WA80 experiment [15] at the CERN SPS. ^{16}O- and ^{32}S-induced reactions were selected for centrality by requiring less than 30 % of the total beam energy to be measured in the Zero-Degree Calorimeter [16]. For ^{16}O + Au collisions also samples of other centralities have been analyzed. An additional bias is introduced for all data sets by requiring at least one positive pion pair to be detected in the Plastic Ball. This cut also favors central reactions.

Positive pions have been measured using the Plastic Ball detector [14]. A technical summary on the particle identification is given in table 1. Pions were identified both with the $\Delta E - E$-signals and with the delayed signals from the sequential decay to muons and eventually positrons. Details of the analysis procedure can be found in [11].

detector technique	phoswich (CaF$_2$, plastic)
no. of modules	655
identification	$\Delta E - E$ & decay $(\pi^+ \to \mu^+ \nu_\mu \to e^+ \nu_e \bar{\nu}_\mu \nu_\mu)$
resolution σ_Q	≈ 10 MeV
rapidity y_{lab}	-1 – 1
transv. mom. p_T	40 MeV/c – 200 MeV/c
misidentification	$\approx 5\%$

Table 1: Pion identification and acceptance of the Plastic Ball detector [14].

Uncorrelated pair distributions were created using the so-called event-mixing technique. Only events with the same pion multiplicity in the Plastic Ball were combined to form mixed pairs. It has been shown in several publications [7, 17] that distortions of single particle spectra (like e.g. those arising from the Bose-Einstein statistics itself) may naturally lead to distortions in experimentally extracted correlation functions. While it was recommended in [17] to use unsymmetrized pair distributions instead of the product of singles rates, the extraction of such distributions from experimental data is not straightforward. As was emphasized in [7] the singles distributions should be the same for positive and negative pions, so the same arguments apply to both the event-mixing technique and the use of unlike-charged pion pairs for the background distribution. However the calculations in [17] were performed for conditions similar to e^+e^--collisions, while the estimates obtained in [7] show that the distortion effects may not be very severe for the source sizes expected in heavy ion reactions. We will therefore not perform any correction for these effects. This seems to be a good approximation, because there are no residual effects visible in the correlation functions investigated here - e.g. the correlation functions are perfectly flat outside the region of the enhancement.

It was already realized in previous analyses [11] that the positron signal used for the pion identification may lead to problems. Not all decay-positrons are stopped in one detector module. Some may scatter out into a neighboring module causing a fake time signal. If the energy signals in this module accidentally satisfy the cuts used for pion identification, which can arise e.g. from a negative pion, this cross-talk would simulate a positive pion. However, for all these fake pions there exists a module close by, which shows a coincident time signal. By requiring that no pairs are used where the two timing signals are closer than 60 ns all fake pairs could be eliminated.

However, if such a scattering masks a true pair of positive pions, this will also be rejected. This procedure therefore introduces a pair efficiency, which
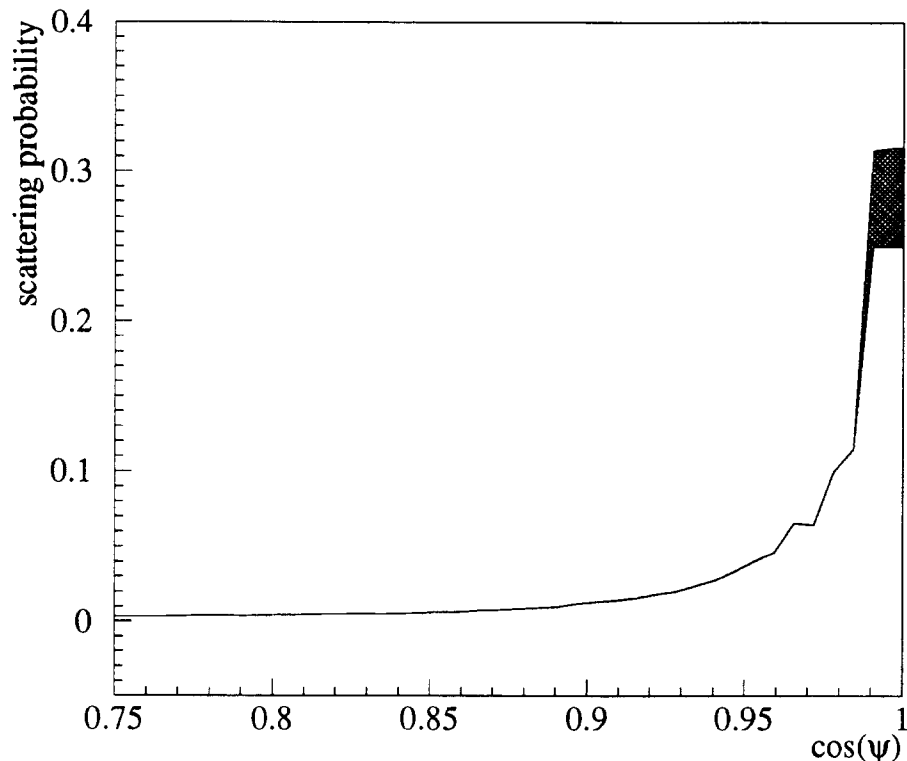
Figure 1: Scattering probability of a positron from a pion decay as a function of the opening angle of the pair of detector modules. The shaded area shows the systematic uncertainty of this probability. The "kinks" in the line are due to the granular structure of the detector.

depends on the relative distance of the detector modules and implicitly on the measured relative momentum. Such an efficiency would lower the correlation function at small relative momenta.

In [11] it was stated that the cross-talk effects are negligible for pair opening angle $\psi > 25°$. Therefore, in the analysis only pairs with larger opening angles were used. While this solves the efficiency problem, it reduces significantly the statistics in the interesting region of small relative momentum.

In the present paper a different approach was used. The probability of a positron faking a time signal was extracted from the data - it can be taken as the number of coincident time signals for a given opening angle normalized to the detector phasespace. Figure 1 shows the extracted scattering probability as a function of the opening angle. From this the pair efficiency, i.e. the ratio of correctly identified positive pion pairs to the true pairs, was calculated. It is observed that the efficiency is only a function of this one variable and

does not depend on global observables like e.g. the particle multiplicity. It is a detector property, which doesn't seem to be influenced by the hit density. Variations in the extracted values for different data samples are found, but no systematic effect for the dependence on multiplicity, target, projectile or the angle θ was seen. These variations are included in the systematic error of the efficiency.

The consequences of the different analysis procedure can be seen by comparing correlation functions obtained with the two different methods. Figure 2 shows an example of such a comparison for the reaction of ^{16}O + Au. The two functions are indistinguishable beyond values of $Q = 50\,\mathrm{MeV}$. For the data with the opening angle cut the statistics is very limited for smaller values of Q. Here one can only say that the data points agree within errors. One should however keep in mind that the shape of the selected region in relative phase space is different depending on whether the angular cut is used or not.

In the present analysis the extreme values of the scattering probability (see figure 1) are used to obtain an estimate of the systematic error due to the efficiency correction.

The Gamow-corrected correlation functions have been fitted with a maximum likelihood method [11] using Gaussian, exponential and double-Gaussian parameterizations as functions of the invariant relative momentum

$$Q = \sqrt{(p^{\mu}_{(1)} - p^{\mu}_{(2)})(p_{(1)\mu} - p_{(2)\mu})}$$

and the longitudinal and transverse components of the relative momentum. This approach is simple, but has the following disadvantages :

1. The strong interaction is ignored.

2. The Coulomb interaction is treated in a local, non-relativistic approximation.

3. The detector resolution is not taken into account.

While the strong interaction may be negligible for heavy ion collisions, it is known that the Coulomb effects deviate from the Gamow approximation for larger source sizes. Also the detector resolution of the Plastic Ball may significantly influence the correlation functions.

In addition to these standard fits the pion correlations have therefore been analyzed by comparing to results of a Monte-Carlo program [18]. This program uses a given phase space distribution of pions to sample the two particle wave functions with symmetrization, Coulomb interaction and s-wave strong interaction phase shifts. Detector acceptance and resolution have been incorporated. The phasespace distributions were created randomly according
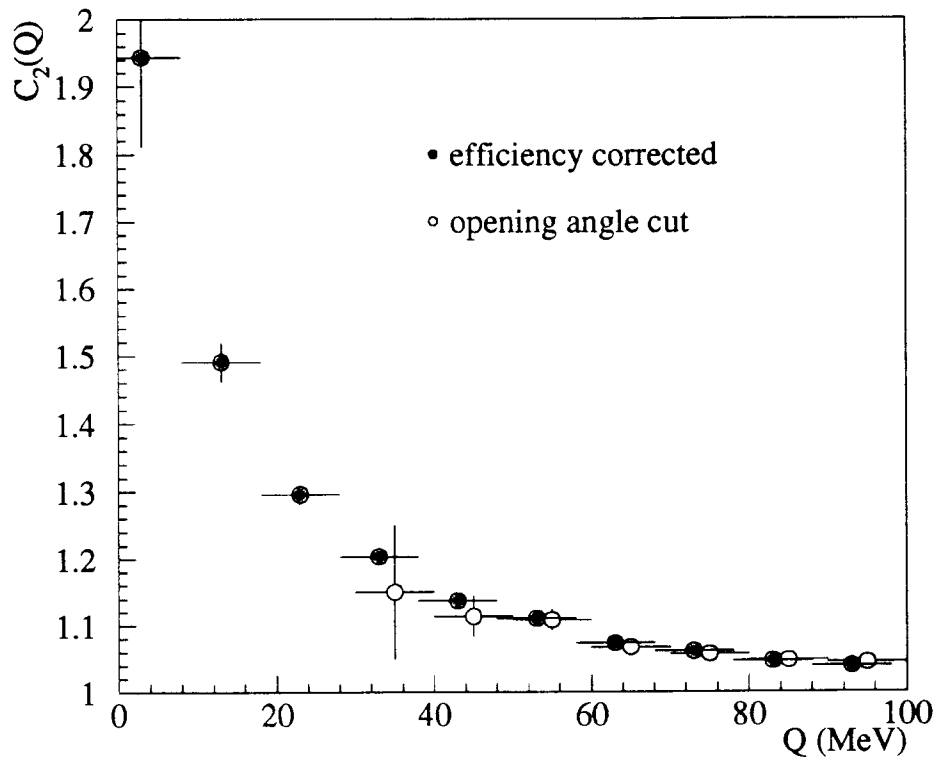
5

Figure 2: Correlation functions for reactions of 200 AGeV ^{16}O + Au obtained with the opening angle cut as in [11] (open symbols) and the efficiency correction used in the present paper (filled symbols). It can be seen that the two functions are compatible in the region of overlap. However only the efficiency corrected correlation functions allow to measure down to low values of the relative momentum Q. The filled symbols are slightly displaced for clarity.

to measured pion spectra and various parameterizations for the source distribution.

Both these approaches rely on the assumption of a static source. We have not studied a dynamical source because of principle and pragmatic reasons:

- The investigation of the dynamics of the source relies on model assumptions about the correlations between space-time and momentum space.

- Current event generators, which claim to describe also the target region at least qualitatively, require very much computing time to deliver results for a reasonable comparison.

6

The static source assumption yields *effective* radii. These require some caution when being interpreted, but this is true for all other approaches, too. It should however be kept in mind, that in the static picture most (if not all) dynamical models would predict effective sources smaller than the geometrical sizes [19, 20, 21].

3 Results

3.1 Standard fits

One-dimensional correlation functions, which are corrected for the Coulomb interaction by the so-called Gamow factor, are displayed in figures 3 and 4. Here data are analyzed as a function of $Q = \sqrt{(p_{(1)}^\mu - p_{(2)}^\mu)(p_{(1)\mu} - p_{(2)\mu})}$. Also shown are Gaussian (2) and exponential (3) parameterizations; for the reactions with the gold target also two-component Gaussians (4) are included.

$$C_2(Q) \equiv 1 + \lambda \exp\left(-\frac{Q^2 R^2}{2}\right) \tag{2}$$

$$C_2(Q) \equiv 1 + \lambda \exp\left(-QR\right) \tag{3}$$

$$C_2(Q) \equiv 1 + \left[\lambda_1 \exp\left(-\frac{Q^2 R_1^2}{4}\right) + \lambda_2 \exp\left(-\frac{Q^2 R_2^2}{4}\right)\right] \tag{4}$$

All functions exhibit the typical Bose-Einstein enhancement for small values of Q. One can see immediately that the Gaussian does not provide a good fit. The exponential gives a much better description of the data - this is confirmed by the log-likelihood values.[1] For p, ^{16}O and ^{32}S + Au the double-Gaussian is still better.

The extracted radius values for the Gaussians are in the range of 4-5 fm; the radius parameters for the exponentials are generally larger. Also the correlation strength λ is slightly higher for the exponentials. The parameter values are listed in table 2.

In [11] a clear, but counterintuitive observation was made: the source radii seemed to decrease with increasing target size. A simultaneous decrease in λ was seen, too. It was already suspected in [11], that this effect was due to a subtle interplay between the measurement of correlations at the limit of the resolution of the detector and the special choice of a fitting function. The simultaneous decrease of both fit parameters may be explained by the following scenarios:

---

[1]The log-likelihood was normalized in such a way, that their numerical values should correspond closely to those expected for a χ^2 function.
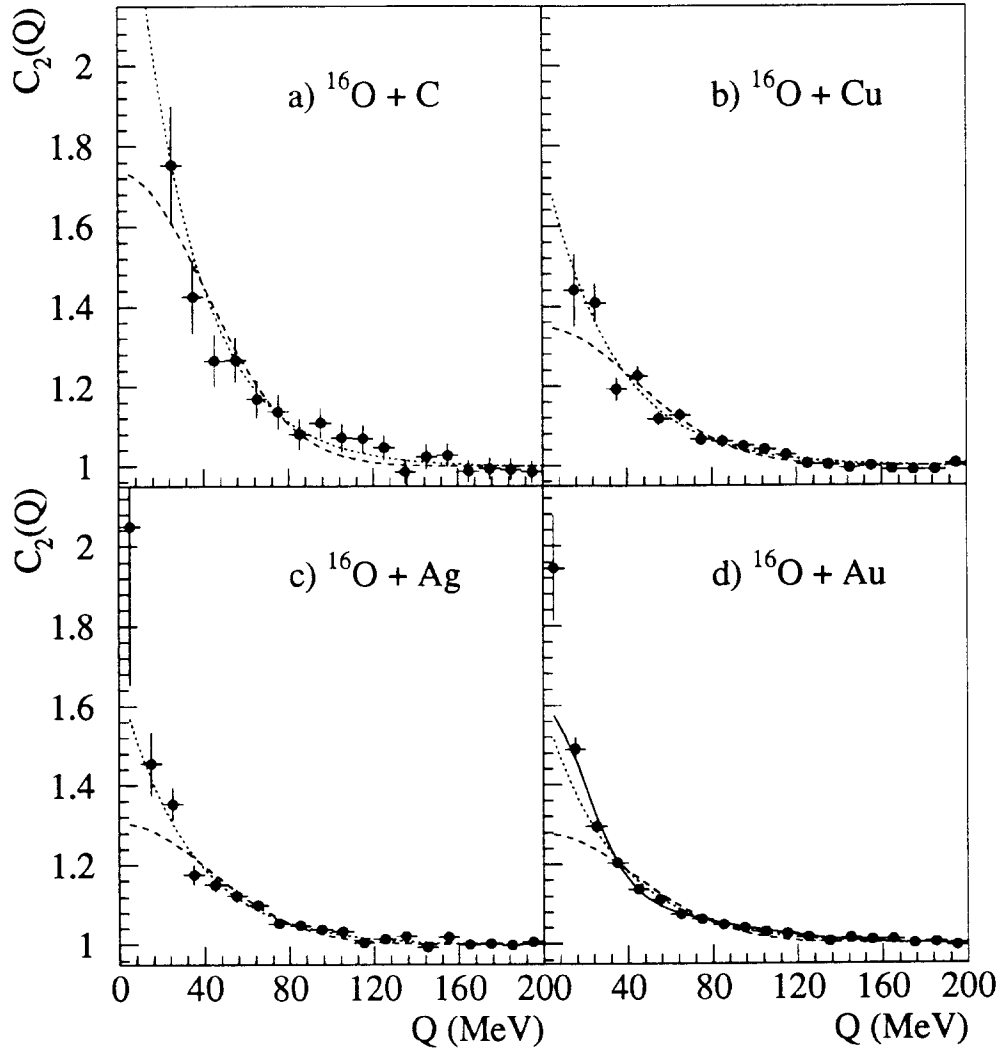
Figure 3: Correlation as a function of Q for reactions of 200 AGeV ^{16}O on various targets (C, Cu, Ag, Au). The experimental data (circles) are efficiency- and Gamow-corrected. As a comparison the best fits of Gaussian (dashed line) and exponential (dotted line) parameterizations are included. The solid line shows a double-Gaussian for ^{16}O + Au. The error bars are statistical only.

8

Figure 4: Correlation as a function of Q for reactions of 200 AGeV ^{32}S with Al and Au and 200 AGeV protons with C and Au. The experimental data (circles) are efficiency- and Gamow-corrected. As a comparison the best fits of Gaussian (dashed line) and exponential (dotted line) parameterizations are included. The solid lines show double-Gaussians for p and ^{32}S + Au. The error bars are statistical only.
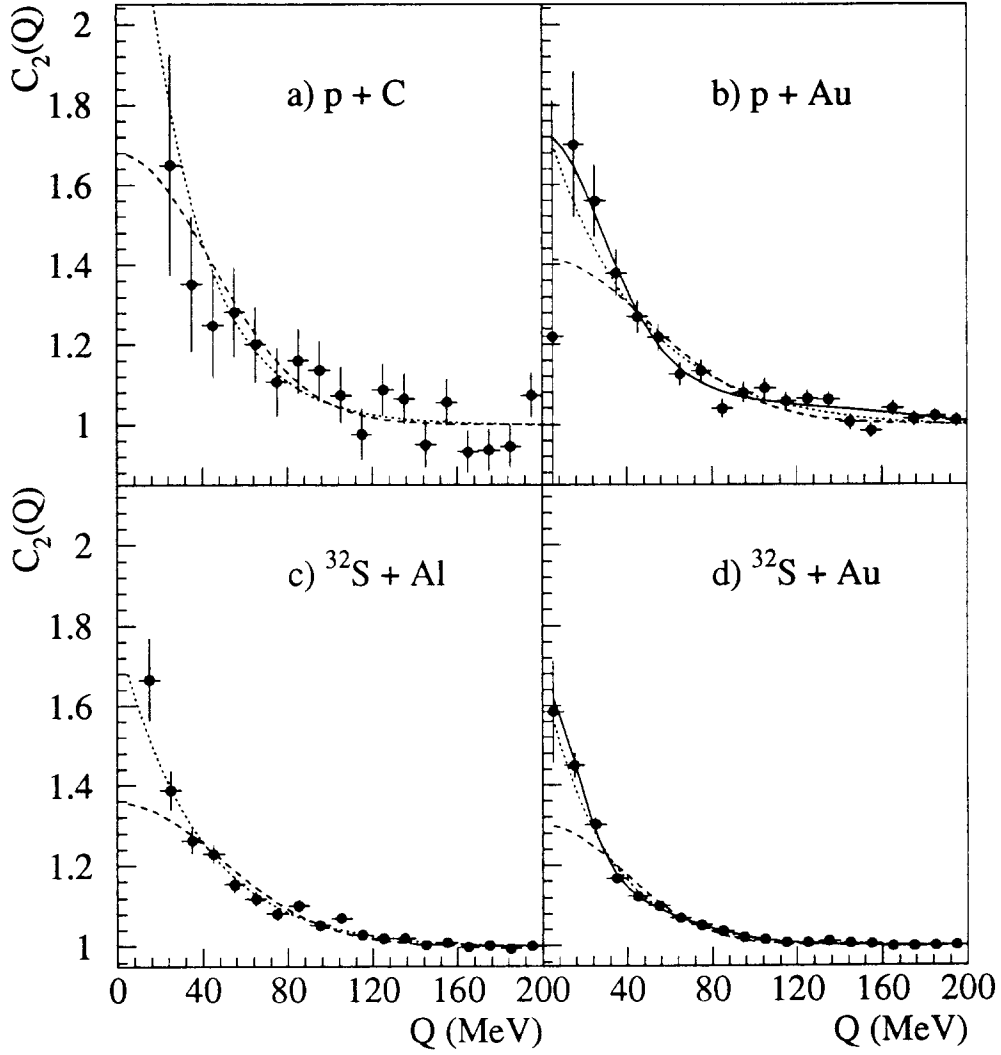
9

The pion emitting source for different systems may change in such a way that a larger fraction of it is effectively hidden at small Q. (This is e.g. the case for pions decaying from long-lived resonances.) In [11] it was shown that a two-component source could simulate the observed effect, if the smaller source stayed the same while the larger one increased for larger targets.

In the present analysis the behavior of the radius parameters has changed. Especially for the larger targets the radius values have increased compared to [11], so that the target dependence is not very striking. This is obviously caused by the better sensitivity of the present analysis at low relative momentum. Still the correlation strength decreases for increasing target mass, which indicates that one still misses part of the correlation function. In addition, for those cases, where statistics allows it, the double-Gaussian yields the best fit.

The results of the two-dimensional fits (Q_T, Q_L) are summarized in table 3. In all cases the transverse and longitudinal radii extracted are very similar and slightly smaller than those extracted from the one-dimensional fits. Again the exponentials work better than the single-Gaussians, and the double-Gaussians provide the best fits.

3.2   Simulation fits

We have seen that, in addition to the caveats already listed in section 2, the fits do not provide a description of the data, which can be easily interpreted. Especially the variation of the strength parameter λ leaves room for speculation and casts doubt on the validity of the radius parameters.

If the observed behavior of the fit parameters is in fact related to a very large source component, this would make the estimate of actual source radii unreliable and would call for a more thorough treatment, especially of the Coulomb interaction and the detector resolution. We have therefore followed another approach, where the pion pairs are simulated according to realistic, observed distributions. The granularity of the Plastic Ball detector, which is to a large extent responsible for the limited resolution, was incorporated as well as the energy resolution. The background of other particles among the pion sample ($\approx 5\%$) and the two-particle efficiency due to the cross-talk discussed above were taken into account.

The wave function of the pion pairs was calculated with a code, which uses the full Coulomb and strong interaction [18]. It should therefore account for deviations of the Coulomb correction due to source size effects.

The evaluation of the correlation function with this Monte Carlo simulation requires much greater computing time than using a simple analytical formula. It is therefore excluded to perform a general fit with standard fitting algorithms, especially for more than one free parameter. We have chosen to analyze the data only as a function of Q. A set of correlation functions for a

10

range of source sizes was calculated, where symmetrical Gaussian:

$$f(r_i) \propto \exp\left(-\frac{r_i^2}{R^2}\right)$$

and Lorentzian source shapes:

$$f(r_i) \propto \frac{1}{1 + (r_i/R)^2}$$

were employed ($r_i = x, y, z, t$). For technical reasons the Lorentzian source distributions were truncated at $r_i = \pm 10R$. This gives integrable distributions and allows to obtain RMS-values of the radii for comparison. While the value of the RMS depends on the actual cutoff used, this is not so important for our purpose - the truncated Lorentzian should just be taken as one example of a distribution with a long tail. The time and the three space components were taken to be equivalent in the source distribution. The strength of the correlation was set to one. This leaves us with only one free parameter (a radius) for each calculation.

The simulated correlation functions were compared to the experimental functions and χ^2-values were obtained. The optimum parameter was estimated using a quadratic interpolation of the χ^2 around the minimum.

The radius parameters (as well as the RMS-radii) are given in table 4. A comparison of these simulated correlation functions with the experimental data is shown in figures 5 and 6. In contrast to the previous figures the experimental functions are not Gamow-corrected in these plots, since the calculations include the Coulomb interaction.

Both from the figures and the table one can see that in most cases the Lorentzian source results in a better description of the data. This is not surprising in view of the results of the standard fits, because a Lorentzian source corresponds to an exponential shape for the standard fit. The Lorentzian always yields slightly larger RMS-radii because of its long tail towards large distances.

The χ^2-values for these simulations are comparable to those obtained for the fits. The extracted radius values are however significantly larger in most cases. This is related to the fact that our simulations have been performed assuming a correlation strength $\lambda = 1$. The extracted radii are closer in cases where the λ-value of the standard fit is close to one. For those systems, where a very small value of λ is reported from the standard fits, the radius from the simulation is much larger. The large source in the simulation accounts partly for a component of the source, which would not be identifiable through the fit and would only reduce the apparent strength, as observed.

11
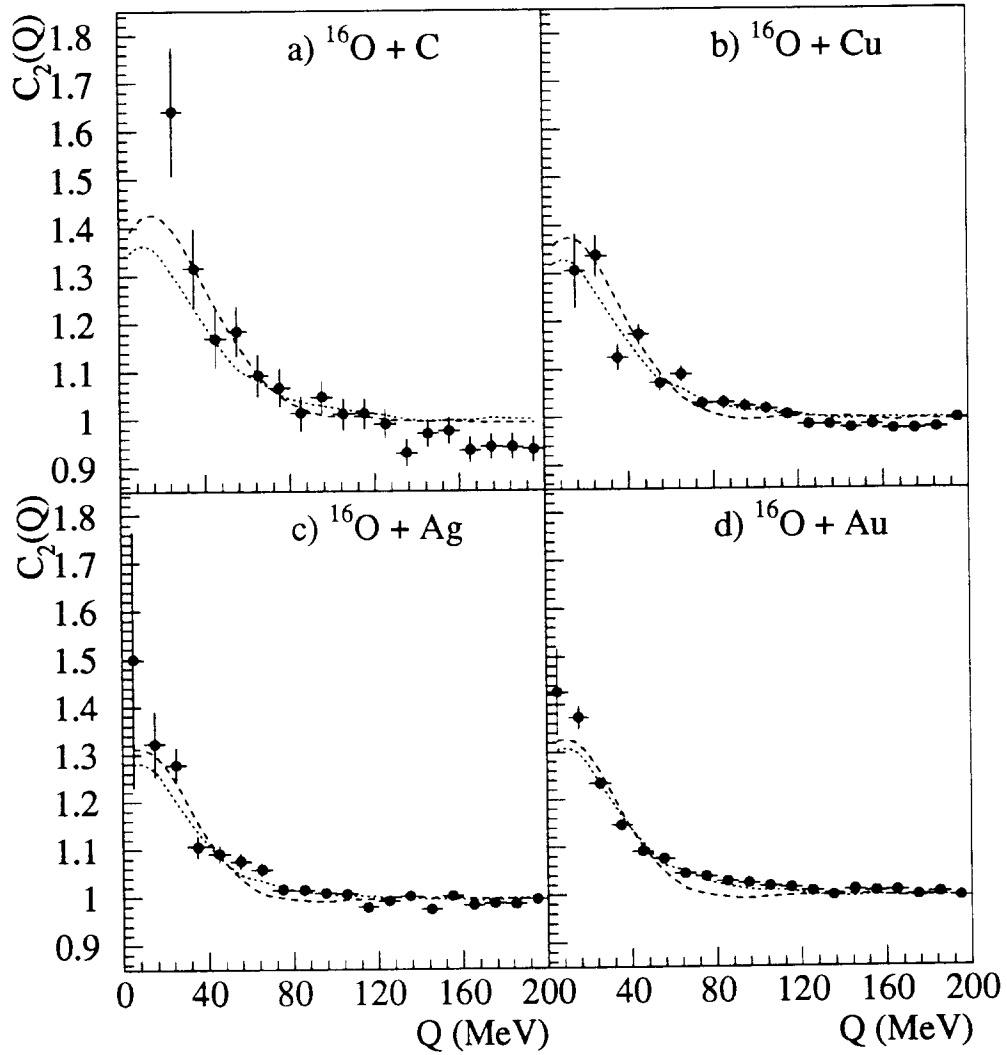
Figure 5: Correlation as a function of Q for reactions of 200 AGeV ^{16}O on various targets (C, Cu, Ag, Au). The experimental data (circles) are corrected for pair efficiency, but not for Coulomb effects. As a comparison the best fits from the Monte Carlo calculations using a Gaussian (dashed line) and a Lorentzian (dotted line) source are included. The error bars are statistical only.

Figure 6: Correlation as a function of Q for reactions of 200 AGeV ^{32}S with Al and Au and 200 AGeV protons with C and Au. The experimental data (circles) are corrected for pair efficiency, but not for Coulomb effects. As a comparison the best fits from the Monte Carlo calculations using a Gaussian (dashed line) and a Lorentzian (dotted line) source are included. The error bars are statistical only.
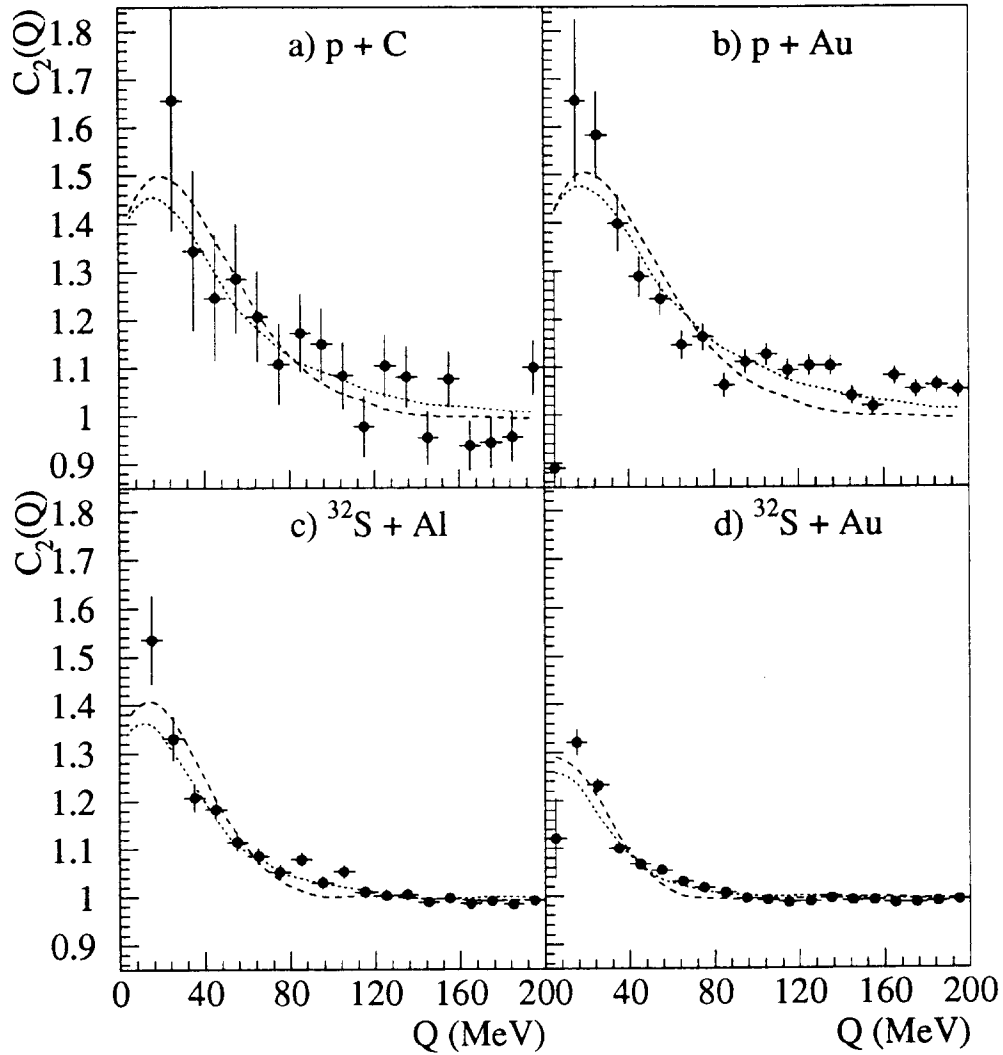
The results of the simulation can be regarded as compatible with those of the fits, however, both from the more thorough treatment of the Coulomb interaction and detector resolution and the consistency of the results we have more confidence in the simulation.

The target dependence follows an expected trend: The radii increase with increasing target size. For the largest targets the RMS-radii reach values larger than 10 fm.

For the system 200 AGeV ^{16}O + Au the centrality dependence of the correlations was studied in addition. The centrality was estimated from the forward going energy, which was then used to calculate the number of participants. Five different centrality classes were used. The results are summarized in table 5. It can be seen that the radii increase with increasing centrality.

3.3   The correlation strength

The assumption that the correlation strength $\lambda = 1$ seems to be well justified because, especially in the target region, pion pairs should dominantly come from two different binary collisions. For coherence to occur one would therefore need to invoke exotic phenomena like e.g. a condensate.

In addition, detection efficiencies have been included in this analysis. There is however at least one other mechanism, which should reduce the apparent strength: the contribution from the decay of long-lived resonances. These simulate a very large source, which is related to the resonance lifetime and is not resolvable in this analysis. A source much larger than 20 fm is indistinguishable from a reduced correlation strength.

As the effort to fit simultaneously both radius and strength is very demanding, we have used only one system (200 AGeV ^{16}O + Au) to estimate the influence of the strength parameter. We have obtained optimal radius values for $\lambda = 0.25, 0.5, 0.75, 1$. The values are given in table 6.

There is a clear correlation between λ and R, a relation that is also known for fits of analytical functions ([6]). The best fits are obtained with the Lorentzian source for values of λ of 0.5 or 0.75. The RMS-radius is still ≈ 10 fm.

While these calculations provide the best χ^2 for this system, it is highly probable that another shape of the source distribution may yield a similar description assuming $\lambda = 1$, as in fact a source shape with a very large component would be experimentally equivalent to the assumption of a smaller value of λ. As one can see from figure 7, where the different simulations for a Lorentzian are compared to the data, none of these correlation functions describes the data perfectly. While the simulation with a small λ does not fit in the region of small Q, it provides a good description at $Q \approx 100$ MeV. The

calculation for $\lambda = 1$ works better for small Q, but has a small discrepancy at more intermediate Q, which is however important because of the small statistical error of the data in this region.

The question, whether a smaller value of λ should be used, can not be decided in this analysis. We must note however that the effect of a smaller λ-parameter might lead to a $\approx 20\%$ reduction in the radii. We would expect this effect to be smaller for the other systems, as the λ-parameter from the fits is smallest for (200 AGeV ^{16}O + Au).
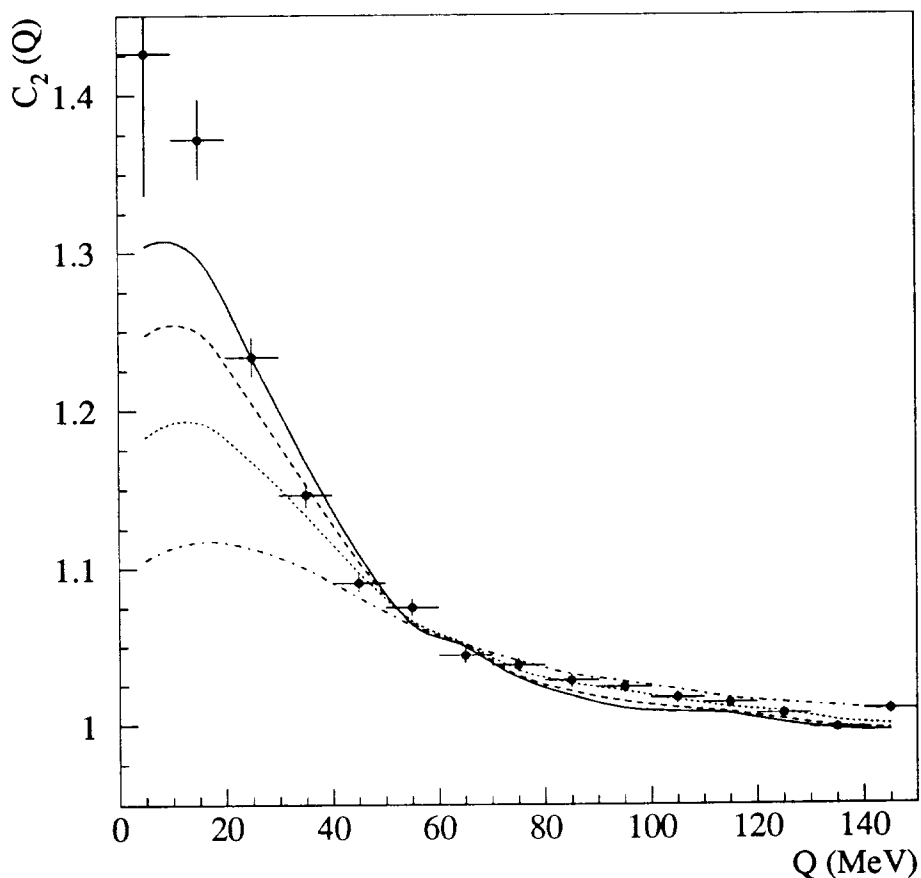
Figure 7: Correlation function for 200 AGeV ^{16}O + Au with simulations assuming different values of the correlation strength. The solid line shows $\lambda = 1$, the dashed line $\lambda = 0.75$, the dotted line $\lambda = 0.5$ and the dash-dotted line $\lambda = 0.25$.

The comparatively large χ^2-values of even the best fits shown here in-

15

dicate that the optimal description of the data has not been found. This will not be attempted, as the freedom to choose a specific distribution is very large and the effects of small changes in the shape on the effective radii should not be very important.
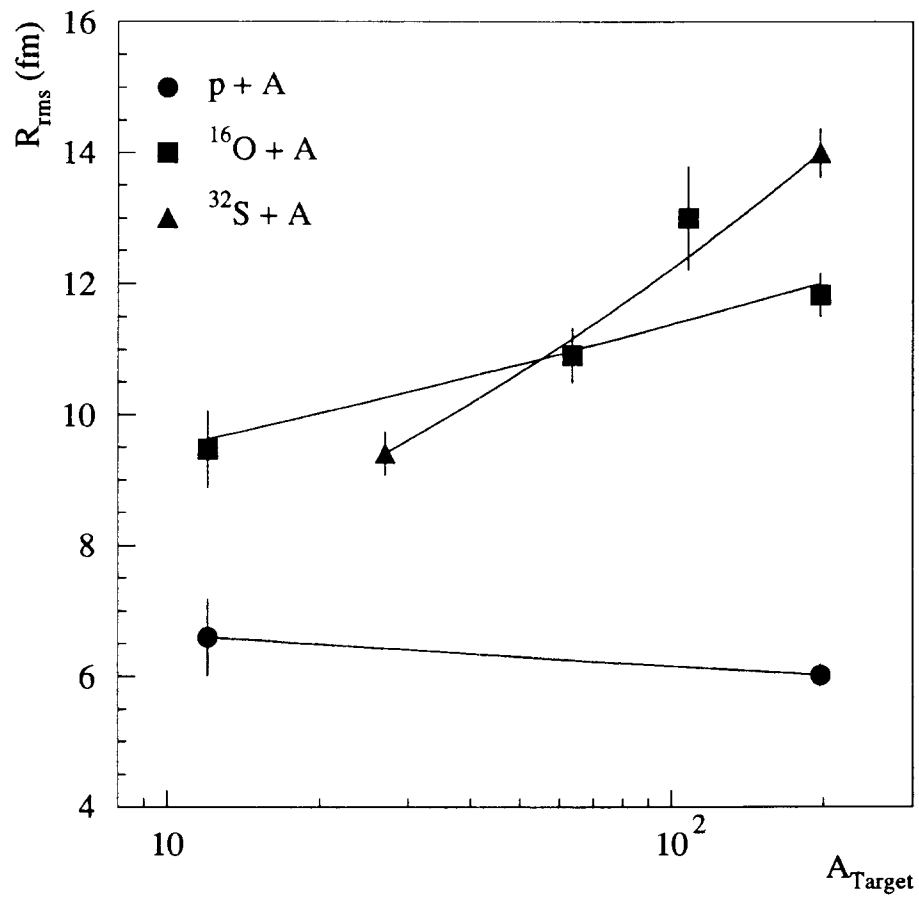
Figure 8: RMS-radii extracted from simulations using a Lorentzian source shape as a function of the target mass. The lines show fits of a power law for the three different projectiles.

4 Discussion

The target dependence of the extracted radii[2] is displayed in figure 8. While there is a clear increase of the radii with target mass for ^{16}O- and ^{32}S-induced reactions, there is no such dependence for p-induced collisions. In figure 8 a power law $R \propto A^\alpha$ was fitted to the target dependence. The p-induced reactions yield $\alpha = -0.03 \pm 0.04$. For 200 AGeV ^{16}O + A and ^{32}S + A one obtains $\alpha = 0.08 \pm 0.03$ and $\alpha = 0.20 \pm 0.03$, respectively.
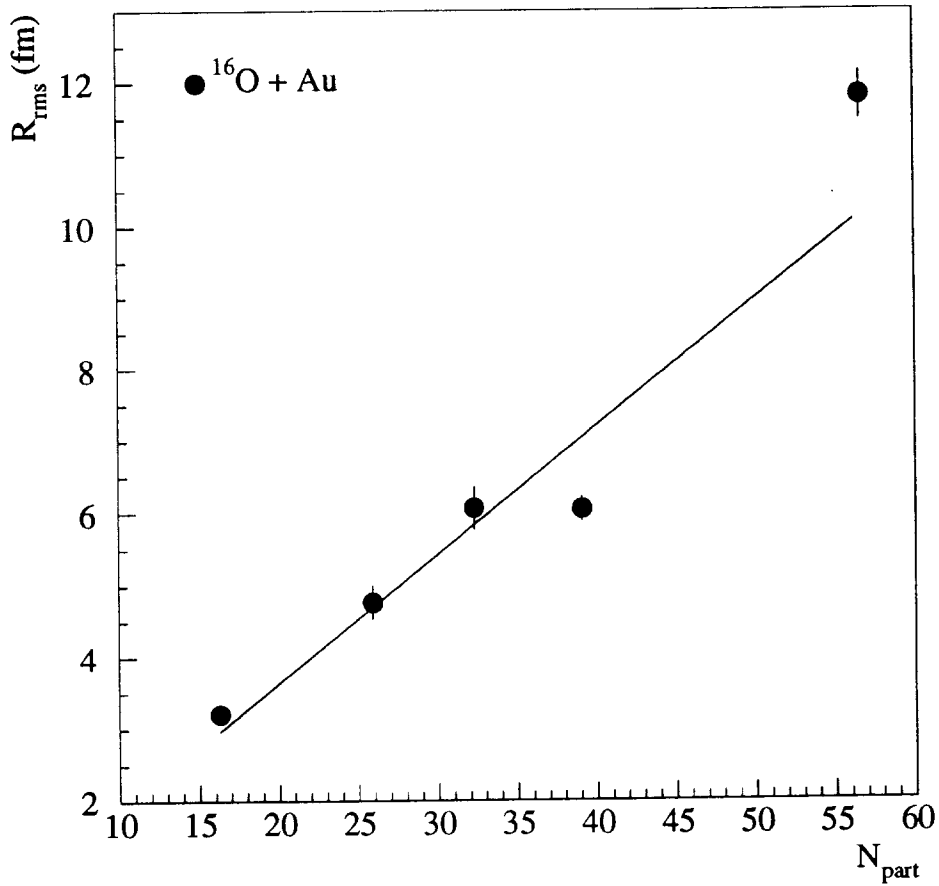

Figure 9: RMS-radii extracted from simulations using a Lorentzian source shape as a function of the average number of participants for reactions of 200 AGeV ^{16}O + Au. The lines show a fit of a power law.

---

[2]In the following we will use the Lorentzian source with $\lambda = 1$ unless stated differently.

A simultaneous fit to ^{16}O- and ^{32}S-data yields $\alpha = 0.14 \pm 0.02$. The target dependence appears to be relatively weak compared to e.g. the geometrical target radius.

Both from the weak target dependence[3] and the discrepancy between the absolute values and the geometrical size of the target nuclei one can conclude that the target size plays only a minor role in determining the pion source size. This has to be compared to the WA80 analysis in [22], where it was found that the source of protons in the target region is very closely related to the size of the target nucleus. Obviously the mechanisms involved in pion and proton emission in the target region are different.

The centrality dependence for 200 AGeV ^{16}O + Au is shown in figure 9. One observes a significant increase of the radii with increasing number of participants - a fit results in a power $\alpha = 0.99 \pm 0.07$. This can not be understood purely from the geometry of the interaction region (fireball), because one would expect $\alpha \approx 1/3$, but shows a more prominent dependence on the "violence" of the collision. Peripheral ^{16}O + Au collisions seem to have a similar source size to p + A collisions, while for central heavy ion reactions the source size is considerably larger.

For the simulations we have assumed that the source is at rest in the laboratory (=target) frame, which seems to be reasonable for measurements in the target fragmentation region. If the source itself, or part of it, is moving in the laboratory frame, the interpretation is more complicated. In the appendix a simple estimate on the possible effects of Lorentz transformation is given - it is shown that effective radii might be enlarged by as much as a factor 3.6. This would however contradict the indication from the standard fits for a source, which is spherically symmetric in the lab. This would correspond to a rather moderate correction. Also the centrality dependence would not be explained: It is unlikely that the transformation effects enter only for central collisions.

In addition, data from the NA35 collaboration on pion interferometry for similar reactions [23] indicate that pions observed at small rapidities are also emitted from a source at small y. One can conclude that Lorentz transformation should only have very little influence on the results shown here.

A direct comparison of these data to NA35 is difficult, because the corresponding rapidity regions do not overlap (they measure for $y_{lab} > 0.5$). A look at their most backward region reveals that the mean values of their outward and sideward radii obtained from Gaussian fits are similar to the transverse radii given by the standard Gaussian fits to our data - both are in the range of 4-5 fm. While this may be reassuring, we have to emphasize again, that we believe the simulation fits to be more reliable. The Gaussian radii extracted there e.g. for ^{16}O + Au and ^{32}S + Au are almost a factor of

---

[3]The target dependence would even be weaker, if the effects of $\lambda < 1$ were included.

two higher than the standard Gaussian fits.

5   Conclusions

Correlations of positive pions were measured in the target rapidity region for central reactions of protons, ^{16}O and ^{32}S with various targets. A new efficiency correction for pion pairs was extracted and applied to the correlation analysis.

Standard fits with analytical functions have been performed on Gamow-corrected correlation functions. The parameters extracted from these fits exhibit the following features:

1. In most cases exponentials provide a better fit to the data than single-Gaussians.

2. The radius parameters extracted show no significant dependence on projectile or target. The values are $\approx 4 - 5$ fm for the Gaussian fits and $\approx 6 - 7$ fm for the exponential fits.

3. The apparent correlation strength decreases with increasing target size.

4. A double-Gaussian yields the best fit for the heaviest target. The second component has radius values of $\approx 10 - 15$ fm.

5. A two-dimensional analysis shows no directional dependence of the radii.

It is obvious that the Plastic Ball detector is at its limit for such large sources. For reliable estimates of the source size it is therefore indispensable to incorporate the detector resolution, which was done with a Monte-Carlo simulation. This simulation also takes into account more realistically the effects of final-state interactions. The results of these simulations are:

1. In most cases the Lorentzian source describes the data much better than a Gaussian. The extracted radii are larger than the geometrical size of the nuclei involved.

2. There is a weak increase of the radii with the target size for central heavy ion reactions. The RMS-radii reach values larger than 10 fm.

3. Radii for ^{16}O + Au reactions show a strong centrality dependence.

4. Proton-induced reactions show source sizes similar to peripheral heavy-ion reactions.

19

5. Simulations assuming a small correlation strength yield smaller radius values, which are however still of the order of 10 fm.

The simulations shown here still do not provide an optimum description of the data. It is beyond the scope of this paper to find the best possible source distribution for all the various reaction systems, because of the very high computational effort. However, the approach used is clearly more appropriate than fitting simple analytical functions to Gamow corrected data.

The analysis has shown that the pion source in the target region is much larger than the geometrical size of the nuclei. Lorentz-transformation effects are not very likely to explain these radii. Some of the observed effect may be related to resonance production of the pions. This would have to be investigated with a more detailed Monte-Carlo.

6 Acknowledgments

A   Appendix

The Lorentz-transformation properties of the source sizes are determined by the behavior of the measured momenta.[4] Pions with rapidity y in a frame with y_F have a momentum:

$$p = m_T \cdot \sinh(y - y_F).$$

A small variation of the momentum is then:

$$dp = m_T \cdot \cosh(y - y_F) \cdot dy.$$

So for pions emitted from a source at y_S and observed in a frame at y_O the ratio of (longitudinal) source sizes in the different frames should be:

$$\frac{R_O}{R_S} = \frac{dp_S}{dp_O} = \frac{\cosh(y - y_S)}{\cosh(y - y_O)}.$$

This formula reduces in two limiting cases:

---

[4]We will consider only the component of the momentum parallel to a Lorentz boost.

1. $y \approx y_S$:

$$R_O = R_S / \cosh(y - y_O) \quad \text{and}$$

2. $y \approx y_O$:

$$R_O = R_S \cdot \cosh(y - y_S).$$

It can be easily seen that case 1 leads to a contraction, while in case 2 an elongation is observed.

Let us assume (for comparison to our results) that the source was moving in the laboratory with $y_{lab} = 2.5$. The rapidities of the pions and the observer are both close to 0. Then the longitudinal component of the radius would appear Lorentz-elongated in the lab:

$$R_L^{lab} = R_L^{cm} \cdot \cosh(y_{lab}),$$

which would correspond to a factor of ≈ 6.

The transverse size would be unaffected, so the average radius would be:

$$R_{RMS}^{lab} = \sqrt{\left[R_L^{cm} \cdot \cosh(y_{lab}) \right]^2 + 2 R_T^2}.$$

For a source, which is spherically symmetric in the center of mass, this leads to:

$$
\begin{aligned}
R_{RMS}^{lab} &= R_{RMS}^{cm} \sqrt{\frac{1}{3} \left[2 + \cosh^2(y_{lab}) \right]} \\
&\approx 3.6 \cdot R_{RMS}^{cm}.
\end{aligned}
$$

This is about the maximum effect one would expect from Lorentz transformation.

However we have information from the two-dimensional fits, that the source appears to be symmetric in the laboratory system. This would rather lead to:

$$
\begin{aligned}
R_{RMS}^{lab} &= R_{RMS}^{cm} \sqrt{\frac{3}{2 + \cosh^{-2}(y_{lab})}} \\
&\approx 1.2 \cdot R_{RMS}^{cm},
\end{aligned}
$$

a more moderate modification of the radii, which would not account for the large measured values.

21

proj.	^{16}O			
targ.	C	Cu	Ag	Au
Gaussian fits				
R^{Gauss} (fm)	5.03±0.33	4.47±0.19	4.80±0.24	4.74±0.25
λ^{Gauss}	0.79±0.15	0.38±0.04	0.33±0.04	0.32±0.04
$\chi^2_{\mathcal{LF}}/\nu$	67/35	89/36	87/37	470/37
exponential fits				
R^{exp} (fm)	7.26±0.52	6.31±0.32	6.43±0.39	6.21±0.40
λ^{exp}	1.90±0.45	0.86±0.12	0.75±0.12	0.68±0.09
$\chi^2_{\mathcal{LF}}/\nu$	43/35	69/36	57/37	166/37
double-Gaussian fits				
$R^{(1)}$ (fm)	-	-	-	2.93±0.15
$\lambda^{(1)}$	-	-	-	0.35±0.02
$R^{(2)}$ (fm)	-	-	-	12.5±0.9
$\lambda^{(2)}$	-	-	-	0.49±0.06
$\chi^2_{\mathcal{LF}}/\nu$	-	-	-	89/35
proj.	p		^{32}S	
targ.	C	Au	Al	Au
Gaussian fits				
R^{Gauss} (fm)	4.60±0.49	4.03±0.25	4.38±0.22	5.39±0.24
λ^{Gauss}	0.71±0.21	0.45±0.08	0.44±0.06	0.33±0.04
$\chi^2_{\mathcal{LF}}/\nu$	48/35	83/37	58/36	216/37
exponential fits				
R^{exp} (fm)	7.42±0.76	4.68±0.33	5.63±0.30	7.39±0.42
λ^{exp}	2.12±0.91	0.87±0.15	0.86±0.11	0.78±0.11
$\chi^2_{\mathcal{LF}}/\nu$	42/35	57/37	48/36	77/37
double-Gaussian fits				
$R^{(1)}$ (fm)	-	1.23±0.42	-	4.07±0.16
$\lambda^{(1)}$	-	0.39±0.08	-	0.42±0.02
$R^{(2)}$ (fm)	-	8.34±0.73	-	15.5±1.0
$\lambda^{(2)}$	-	0.56±0.08	-	0.44±0.07
$\chi^2_{\mathcal{LF}}/\nu$	-	39/35	-	51/35

Table 2: Extracted correlation parameters for one-dimensional fits as a function of Q. Given are results of Gaussian, exponential and double-Gaussian fits including statistical and systematic errors added in quadrature.

22

proj.	^{16}O			
targ.	C	Cu	Ag	Au
Gaussian fits				
R_T^{Gauss} (fm)	4.62±0.46	4.20±0.22	4.01±0.27	4.34±0.18
R_L^{Gauss} (fm)	4.12±0.71	4.26±0.36	4.64±0.36	4.13±0.22
λ^{Gauss}	0.74±0.09	0.37±0.03	0.31±0.03	0.30±0.03
$\chi^2_{\mathcal{LF}}/\nu$	1234/1036	1390/1234	1636/1252	2107/1342
exponential fits				
R_T^{expo} (fm)	-	4.90±0.37	4.57±0.43	5.00±0.27
R_L^{expo} (fm)	-	4.25±0.44	4.48±0.44	3.66±0.25
λ^{expo}	-	0.87±0.09	0.72±0.09	0.66±0.18
$\chi^2_{\mathcal{LF}}/\nu$	-	1374/1234	1608/1252	1890/1342
double-Gaussian fits				
$R_T^{(1)}$ (fm)	-	-	-	2.90±0.17
$R_L^{(1)}$ (fm)	-	-	-	2.34±0.22
$\lambda^{(1)}$	-	-	-	0.35±0.02
$R_T^{(2)}$ (fm)	-	-	-	11.7±1.3
$R_L^{(2)}$ (fm)	-	-	-	11.6±1.0
$\lambda^{(2)}$	-	-	-	0.48±0.06
$\chi^2_{\mathcal{LF}}/\nu$	-	-	-	1742/1339
proj.	p		^{32}S	
targ.	C	Au	Al	Au
Gaussian fits				
R_T^{Gauss} (fm)	-	3.81±0.37	3.84±0.22	4.96±0.21
R_L^{Gauss} (fm)	-	3.67±0.41	3.78±0.28	4.71±0.23
λ^{Gauss}	-	0.45±0.04	0.37±0.03	0.32±0.03
$\chi^2_{\mathcal{LF}}/\nu$	-	1169/1100	1428/1194	1733/1329
exponential fits				
R_T^{expo} (fm)	-	3.94±0.47	4.51±0.38	5.86±0.31
R_L^{expo} (fm)	-	2.86±0.42	3.57±0.35	4.45±0.32
λ^{expo}	-	0.88±0.09	0.85±0.08	0.75±0.09
$\chi^2_{\mathcal{LF}}/\nu$	-	1154/1100	1415/1194	1665/1329
double-Gaussian fits				
$R_T^{(1)}$ (fm)	-	1.44±0.37	-	3.90±0.15
$R_L^{(1)}$ (fm)	-	0.77±0.38	-	3.53±0.20
$\lambda^{(1)}$	-	0.37±0.04	-	0.42±0.02
$R_T^{(2)}$ (fm)	-	7.24±0.76	-	15.2±1.1
$R_L^{(2)}$ (fm)	-	7.42±0.94	-	15.2±1.3
$\lambda^{(2)}$	-	0.54±0.06	-	0.48±0.07
$\chi^2_{\mathcal{LF}}/\nu$	-	1128/1097	-	1600/1326

Table 3: Extracted correlation parameters for two-dimensional fits as a function of Q_T and Q_L. Given are results of Gaussian, exponential and double-Gaussian fits including statistical and systematic errors added in quadrature.

proj.	^{16}O			
targ.	C	Cu	Ag	Au
Gaussian sources				
R^{Gauss} (fm)	5.79±0.28	6.94±0.25	8.54±0.52	8.09±0.23
R^{RMS} (fm)	7.09±0.34	8.51±0.30	10.4±0.6	9.91±0.28
χ^2/ν	97/37	108/38	101/39	486/39
Lorentzian sources				
R^{Lorentz} (fm)	2.26±0.14	2.61±0.10	3.11±0.19	2.83±0.08
R^{RMS} (fm)	9.47±0.59	10.9±0.4	13.0±0.8	11.8±0.3
χ^2/ν	108/37	82/38	79/39	172/39
proj.	p		^{32}S	
targ.	C	Au	Al	Au
Gaussian sources				
R^{Gauss} (fm)	4.35±0.41	4.30±0.13	6.18±0.16	9.32±0.31
R^{RMS} (fm)	5.33±0.50	5.27±0.15	7.57±0.20	11.41±0.39
χ^2/ν	43/37	194/39	85/38	212/39
Lorentzian sources				
R^{Lorentz} (fm)	1.58±0.14	1.44±0.04	2.25±0.08	3.35±0.08
R^{RMS} (fm)	6.60±0.59	6.02±0.17	9.41±0.34	14.00±0.34
χ^2/ν	42/37	102/39	50/38	143/39

Table 4: Extracted parameters from Monte-Carlo simulations for one-dimensional correlations as a function of Q. Given are results assuming Gaussian and Lorentzian source shapes. The errors quoted include both statistical and systematic added in quadrature.

$< N_{part} >$	16.3	25.9	32.3	39.1	56.6
Gaussian sources					
R^{Gauss} (fm)	2.22±0.07	3.48±0.18	4.51±0.21	4.49±0.13	8.09±0.23
R^{RMS} (fm)	2.72±0.08	4.27±0.22	5.52±0.25	5.50±0.16	9.91±0.28
χ^2/ν	90/39	120/39	182/39	287/39	486/39
Lorentzian sources					
R^{Lorentz} (fm)	0.77±0.03	1.14±0.06	1.45±0.07	1.45±0.08	2.83±0.08
R^{RMS} (fm)	3.21±0.11	4.77±0.23	6.07±0.30	6.06±0.17	11.8±0.3
χ^2/ν	41/39	69/39	122/39	156/39	172/39

Table 5: Extracted parameters for one-dimensional correlations as a function of Q for ^{16}O + Au reactions of different centrality characterized by the average number of participants $< N_{part} >$, which was estimated from the forward going energy. Given are results of simulations assuming Gaussian and Lorentzian source shapes. The errors quoted include both statistical and systematic added in quadrature.

λ	0.25	0.5	0.75	1
Gaussian sources				
R^{Gauss} (fm)	4.27±0.08	5.77±0.13	7.02±0.23	8.09±0.23
R^{RMS} (fm)	5.23±0.10	7.07±0.16	8.60±0.28	9.91±0.28
χ^2/ν	204/39	219/39	358/39	486/39
Lorentzian sources				
R^{Lorentz} (fm)	1.53±0.03	2.08±0.05	2.49±0.07	2.83±0.08
R^{RMS} (fm)	6.39±0.13	8.68±0.21	10.4±0.3	11.8±0.3
χ^2/ν	245/39	121/39	126/39	172/39

Table 6: Extracted parameters for one-dimensional correlations as a function of Q for different assumptions on the correlation strength λ (see text). Given are results of simulations assuming Gaussian and Lorentzian source shapes. The errors quoted include both statistical and systematic added in quadrature.

References

[1] M. Gyulassy, S. K. Kauffmann, and L. W. Wilson, Phys. Rev. C **20** (1979) 2267–2292.

[2] R. Hanbury-Brown and R. Q. Twiss, Nature **178** (1956) 1046.

[3] G. Goldhaber et al., Phys. Rev. **120** (1960) 300–312.

[4] M. Deutschmann et al., Nucl. Phys. **B 204** (1982) 333 – 345.

[5] R. M. Weiner, Phys. Lett. **B 232** (1989) 278.

[6] T. Peitzmann, Z. Phys. C – Particles and Fields **55** (1992) 485 – 489.

[7] T. Peitzmann, Z. Phys. C – Particles and Fields **59** (1993) 127–131.

[8] R. Albrecht et al., Z. Phys. C – Particles and Fields **45** (1990) 529–537.

[9] R. Albrecht et al., Z. Phys. C – Particles and Fields **57** (1992) 37–42.

[10] H. Schmidt et al., Nucl. Phys. **A 544** (1992) 449c–454c.

[11] R. Albrecht et al., Z. Phys. C – Particles and Fields **53** (1992) 225–237.

[12] T. Peitzmann et al., Effective source sizes of low rapidity soft particle emission, (1994), in: Proceedings of 2. International Conference on Physics and Astrophysics of the Quark-Gluon Plasma, World Scientific, Singapore.

[13] T. Peitzmann et al., Nucl. Phys. **A566** (1994) 519c–522c, in: Proceedings of Quark Matter 93.

[14] A. Baden et al., Nucl. Instr. and Meth. **203** (1982) 189.

[15] R. Albrecht et al., Study of Relativistic Nucleus-Nucleus Collisions at the CERN SPS, Aug. 1985, preprint CERN/SPSC/85-39 and GSI preprint 85-32.

[16] G. R. Young et al., Nucl. Instr. and Meth. **A 279** (1989) 503–517.

[17] G. F. Bertsch, P. Danielewicz, and M. Herrmann, Phys. Rev. C **49 No 1** (1994) 442–451.

[18] S. Pratt, 1992, private communication.

[19] S. Pratt, Phys. Lett. **53** (1984) 1219–1221.

[20] Y. M. Sinyukov, Nucl. Phys. **A498** (1989) 151c–160c.

[21] T. Csörgő, Bose-Einstein correlations for longitudinally expanding, finite systems, 1994, preprint LUNFD6/(NFFL-7081).

[22] T. C. Awes et al., Z. Phys. C – Particles and Fields **65** (1995) 207–213.

[23] T. Alber et al., Z. Phys. C – Particles and Fields **66** (1995) 77–88.